CARBON 49 (2011) 2615–2623

available at www.sciencedirect.com

ScienceDirect

journal homepage: www.elsevier.com/locate/carbon

Thermomechanical properties of chemically modified graphene/poly(methyl methacrylate) composites made by *in situ* polymerization

Jeffrey R. Potts [a], *Sun Hwa Lee* [b], *Todd M. Alam* [c], *Jinho An* [a], *Meryl D. Stoller* [a], *Richard D. Piner* [a], *Rodney S. Ruoff* [a,*]

[a] *Department of Mechanical Engineering and the Texas Materials Institute, University of Texas at Austin, One University Station C2200, Austin, TX 78712-0292, USA*

[b] *Department of Materials Science and Engineering KAIST, Daejeon 305-701, Republic of Korea*

[c] *Department of Electronic and Nanostructured Materials, MS 0886, Sandia National Laboratories, Albuquerque, NM 87185-0886, USA*

ARTICLE INFO

Article history:
Received 13 December 2010
Accepted 3 February 2011
Available online 22 February 2011

ABSTRACT

The morphology and thermomechanical properties of composites of poly(methyl methacrylate) (PMMA) and chemically modified graphene (CMG) fillers were investigated. For composites made by *in situ* polymerization, large shifts in the glass transition temperature were observed with loadings as low as 0.05 wt.% for both chemically-reduced graphene oxide (RG-O) and graphene oxide (G-O)-filled composites. The elastic modulus of the composites improved by as much as 28% at just 1 wt.% loading. Mori–Tanaka theory was used to quantify dispersion, suggesting platelet aspect ratios greater than 100 at low loadings and a lower quality of dispersion at higher loadings. Fracture strength increased for G-O/PMMA composites but decreased for RG-O/PMMA composites. Wide angle X-ray scattering suggested an exfoliated morphology of both types of CMG fillers dispersed in the PMMA matrix, while transmission electron microscopy revealed that the platelets adopt a wrinkled morphology when dispersed in the matrix. Both techniques suggested similar exfoliation and dispersion of both types of CMG filler. Structural characterization of the resulting composites using gel permeation chromatography and solid state nuclear magnetic resonance showed no change in the polymer structure with increased loading of CMG filler.

1. Introduction

Graphene, a two-dimensional layer of sp^2-bonded carbon atoms, exhibits exceptional physical properties and is being explored for use in a variety of applications [1]. Chemically modified graphene (CMG) platelets, which can be made in bulk quantities from graphite oxide (GO), have been investigated as a composite filler [2,3]. There are three primary methods for producing GO [4], all of which generate a product with a larger interlayer spacing than graphite (0.6–1.2 nm depending on humidity versus 0.34 nm, respectively) and has several oxygen-based functional groups decorating the surface (e.g., carboxylic acids, epoxides, alcohols) [4,5]. This larger interlayer spacing and presence of hydrophilic surface functionalities are both thought to facilitate the exfoliation of layered GO particles into single- or few-layer graphene oxide (G-O) platelets in water and in polar organic solvents [6] via sonication or stirring. GO can also be exfoliated via 'thermal shocking' [7] (i.e., rapid heating including under inert gas) or microwave irradiation [8] to create loosely-stacked,

* *Corresponding author.*
E-mail address: r.ruoff@mail.utexas.edu (R.S. Ruoff).
0008-6223/$ - see front matter
doi:10.1016/j.carbon.2011.02.023

'worm-like' structures that can be directly incorporated into composites via melt compounding as a conductive, graphene-based filler [9–11].

G-O platelets have an identical chemical structure to GO [4] and for certain applications it may be advantageous to restore the conjugated, sp^2 network to render the platelets electrically conductive (for use as a conductive filler, for instance). Chemical reduction of G-O platelets can be achieved using several reductants, including hydrazine, sodium borohydride, and hydriodic acid with acetic acid [4,5,12]. Upon reduction, G-O platelets tend to agglomerate without steric stabilization [13] or increased electronic stabilization [14,15]. Reduction of G-O platelets in the presence of a polymer (e.g., during processing of a polymer composite) has been demonstrated to maintain the dispersion of the chemically reduced G-O platelets (henceforth, RG-O platelets) [16].

In this work, we prepared composites of poly(methyl methacrylate) (PMMA) by *in situ* polymerization, using either G-O or RG-O as filler. We originally attempted to incorporate RG-O powder directly into PMMA via melt compounding; however, the resulting composites showed poor dispersion and much lower mechanical property enhancements than composites made by *in situ* polymerization (data provided in Supplementary Information). In an attempt to facilitate the dispersion of exfoliated CMG filler, we thus turned to an *in situ* solution polymerization approach to produce the composites. Previous work has suggested that GO can be intercalated with monomer or polymer, and that polymerization in the presence of GO can exfoliate the platelets. For instance, an exfoliated composite morphology was observed by intercalation of GO with a poly(ethylene oxide) macroinitiator prior to a solution-based free radical polymerization of methyl methacrylate; however, the GO was not exfoliated at all prior to polymerization [17]. Motivated by these results, we sought to produce composites via *in situ* polymerization with the intent of achieving a homogeneous, isotropic dispersion of monolayer CMG platelets, as such a level of dispersion is thought to be optimal for reinforcement [18]. Moreover, we sought to compare the reinforcing effectiveness of G-O platelets with RG-O platelets in PMMA, as a difference in interfacial adhesion and/or dispersion caused by the different surface chemistries may affect the thermomechanical properties of the composites.

2. Methods

2.1. Materials

SP-1 graphite (Bay Carbon), DMF (Aldrich), hydrazine monohydrate (Aldrich), and benzoyl peroxide (Aldrich) were all used as received. Methyl methacrylate (MMA; Aldrich, 99%) was filtered over alumina powder (Polysciences) to remove the polymerization inhibitor prior to use.

2.2. Fabrication of composites

Graphite oxide (GO) was prepared via a modified Hummers method [19] and dried for a week under vacuum. GO was then suspended in DMF (0.5 mg/ml) and exfoliated by ultrasonication (VWR B2500A-MT bath sonicator) at room temperature. The G-O platelet/DMF suspension was purged with dry nitrogen for 20 min. Filtered MMA monomer (0.2 mol) and benzoyl peroxide initiator (0.6 mmol) were added to the suspension, and then the mixture was heated to 80 °C to promote polymerization (under N_2). The reaction mixture was maintained at 80 °C until the mixture became viscous (typically 6 h). For RG-O/PMMA composites, after the polymerization was completed and while the polymer was in solution, reduction of the graphene oxide was carried out with hydrazine (1 μl per 3 mg GO) at 80 °C for 24 h. The polymer was then coagulated by slowly adding the DMF/PMMA solution to vigorously stirred ethanol (5:1 with respect to the amount of DMF used) and vacuum filtered to collect the product. The filtered composite was washed with ethanol and dried under vacuum for 48 h to obtain dried flakes of composite. For comparison, neat PMMA was made by the same approach, without GO or hydrazine. For dynamic mechanical testing, the composite flakes were then ground into powder by mortar and pestle and then pressed using a hydraulic hot press (Fred S. Carver, Inc.) at 3.5 MPa and 220 °C for 10 min, resulting in films of approximately 0.20 mm thickness. Composites were also processed by injection molding for tensile testing experiments. Due to the configuration of the molding equipment available to us, the composite flakes (~3 g per specimen) were fed into a twin-screw DSM microcompounder (mixing chamber volume 5 ml) prior to injection molding, despite the filler already being dispersed. For all microcompounded composite samples (only those which were injection molded), the melt mixing temperature was 220 °C, with a screw speed of 100 rpm. The flakes were fed into the mixing chamber with the melt immediately flowing into a mold barrel at 230 °C and then finally injected into an ASTM D638 – Specimen Type V mold at 50 MPa and 100 °C. After processing, all samples were placed in a desiccator to dry at room temperature for 48 h prior to testing.

2.3. Thermomechanical analysis

The viscoelastic response of the composites was measured using dynamic mechanical analysis (DMA Q800, TA Instruments). Strips of uniform width (~5 mm) were cut from the hot-pressed film (thickness of ~0.2 nm) using a razor blade. For fixed-frequency temperature scans, dynamic loading was applied at 1 Hz at 0.02% linear strain with a 0.01 N tensile force preload and a temperature ramp rate of 2 °C/min. DSC (Mettler Toledo) was performed using a ramp rate of 10 °C/min under flowing N_2. TGA (TGA4000, Perkin Elmer) was used to observe changes in thermal degradation behavior versus the neat polymer, using a ramp rate of 10 °C/min with N_2 as the sample purge gas. For mechanical testing of the injection molded composite samples, a single pre-wired resistive strain gage (Vishay, #307441) was bonded to the thin section of the specimen. Tensile testing was performed using an Instron machine using a strain rate of 1%/min.

2.4. CMG platelet characterization

AFM images were recorded on a Park Scientific AutoProbe CP/MT (MultiTask) instrument with scans obtained in contact

mode. Elemental analysis by combustion was performed by Atlantic Microlab, Norcross, GA, USA.

2.5. Composite morphological characterization

Wide-angle X-ray scattering (WAXS) studies were done using a Philips X-PERT diffractometer using Cu Kα radiation. A generating voltage of 40 kV and a current of 30 mA was used, with a 2 s dwell time. Transmission electron microscopy (TEM) and scanning electron microscopy (SEM) were used to image the morphology of the composites. For TEM, injection molded composites were microtomed to slices of 50–90 nm thickness using an ultra45 diamond blade (Leica Ultracut UCT, Reichert Inc.) and dropped onto 300 mesh copper TEM grids (Ted Pella). The TEM images were acquired on a JEOL 2010F at 120 keV. SEM samples were prepared by sputter coating fractured compression molded samples using a 6 nm coating of iridium metal deposited in an Ar atmosphere. Images were acquired using a FEI Quanta-600 FEG Environmental SEM at 5 keV and 10^{-5} torr.

2.6. Spectroscopy and gel permeation chromatography

^{1}H and ^{13}C solution NMR was performed using a Bruker DRX400 at 399.97 and 100.54 MHz, respectively. Neat, as-made PMMA and composites were dissolved in $CDCl_3$ (~5 mg/ml) and spectra obtained at 50 °C using a 5 mm broadband probe at 50 °C using standard pulse sequences. The ^{1}H and ^{13}C chemical shifts were all referenced to residual solvent resonances within the $CDCl_3$ solvent. Solid state ^{13}C magic angle spinning (MAS) NMR was carried out on the neat PMMA and CMG/PMMA composites using a Bruker Avance400 at 100.62 MHz. Spectra were obtained using a standard cross polarization (CP) MAS sequence with variable contact times, at room temperature with spinning at speeds between 4 and 10 kHz. The ^{13}C chemical shifts were referenced to a secondary standard glycine setting the carbonyl resonance at 176.0 ppm with respect to TMS, $\delta = 0$ ppm. FT-IR measurements were obtained using a Perkin–Elmer BX spectrometer. GPC measurements were made at ambient temperature on a home-built system equipped with a Waters Model 510 HPLC pump, two fluorinated polystyrene columns arranged in series, and a Waters 486 Tunable Absorbance Detector ($\lambda = 450$ nm). Molecular weight and polydispersity data are reported relative to polystyrene standards in tetrahydrofuran (THF).

3. Results and discussion

GO was produced by a modified Hummers method and was determined to have a C:O ratio of 1.24 (including contribution from water) as measured by elemental combustion analysis. GO was sonicated in DMF at 0.5 mg/ml for 1 h to create a suspension of G-O platelets. It has been previously reported that G-O can form a stable dispersion in DMF [20]; however, even at 0.5 mg/ml, some sedimentation was observed in the suspension after sitting overnight. Atomic force microscopy (AFM) was conducted on the dried-down platelets after deposition of a diluted G-O suspension onto a mica substrate (Fig. 1). Based on AFM, the suspensions made by sonication in DMF consisted of mostly single-layer G-O platelets, along with some larger multi-layer platelets and also larger particles that were not exfoliated. The single-layer platelets showed a large range of lateral dimensions, ranging from microns to tens of nanometers (Fig. 1). Thus, AFM suggests that mostly single-layer platelets were dispersed into the polymer, although restacking could potentially occur.

In this study, the G-O platelets dispersed in the polymer solution were reduced with hydrazine monohydrate prior to precipitating the polymer out of solution. As previously mentioned, reduction of G-O platelets in the presence of a polymer has been reported to stabilize the platelets against agglomeration [16]. Indeed, this was found to be the case at lower loadings, based upon our analysis of filler dispersion as presented below. It was also of interest to characterize the degree of reduction achieved by hydrazine in the presence of the polymer, as well as reduction as a result of high-temperature processing (molding and compounding steps). To characterize this, the composites were re-dissolved in DMF and the CMG filler was separated from the polymer by centrifugation followed by decanting and vigorous washing to remove all traces of polymer from the CMG surface. TGA scans of these products showed that both hydrazine treatment and high-temperature processing resulted in the reduction of the G-O platelets, as also suggested by inspection of the composite powders (Supplementary Information, Fig. S1).

The exfoliation of the platelets and the level of platelet dispersion achieved in the composites were probed by TEM and wide-angle X-ray scattering (WAXS). TEM images of microtomed sections of the composites are shown in Fig. 2. While AFM analysis of the G-O dispersion suggests single-layer platelets may be dispersed in the matrix, they were not directly observed in our TEM analysis. Many few-layer platelets were observed and were sparsely dispersed throughout the matrix, with a wide distribution of lateral dimensions: many had lengths of hundreds of nanometers, while other platelets appeared to be several microns long. The ultrasonication process used to exfoliate GO also fragments the platelets, and is likely responsible for the small lateral dimensions of many of the platelets [4]. No difference in the level of filler dispersion or exfoliation was observed between G-O and RG-O-filled composites at 0.5 wt.%, suggesting that at low loadings the reduction process does not lead to significant agglomeration of the platelets. However, at higher loadings (4 wt.%), the composites appeared to show an increased number of multi-layer platelets with a larger average thickness (lower aspect ratio). Low magnification TEM images clearly showed orientation of the multi-layer platelets in the matrix, likely due to the injection molding process.

For both G-O and RG-O filled composites, nearly all of the platelets showed a crumpled or wrinkled conformation, with some multi-layer platelets showing a corrugated structure (Supplementary Information, Fig. S4). Although graphene-based fillers can be imaged in TEM without staining, contrast was often very low, and thus it was a challenge to ascertain the level of dispersion in the composite just from TEM observation, due to the difficulty of observing few-layer platelets at lower magnification. WAXS was performed to further analyze the state of dispersion of the composite (Fig. 3). The scattering intensity profile revealed no presence of diffraction peaks

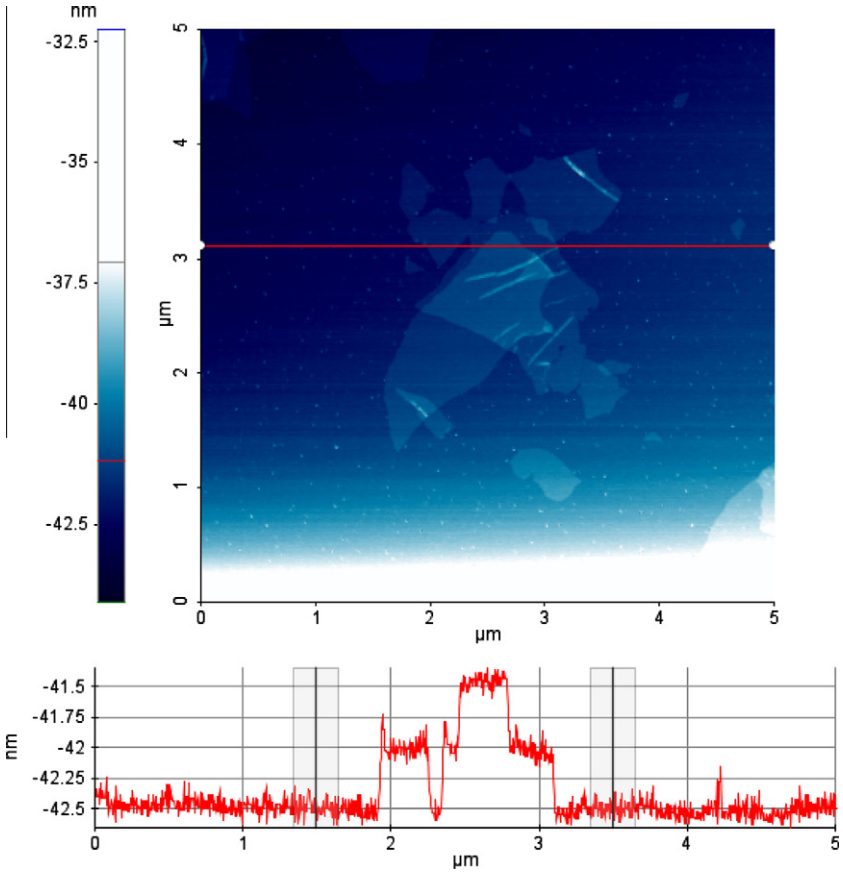

Fig. 1 – Atomic force microscopy scans of dried-down platelets on freshly-cleaved mica revealed the presence of single-layer platelets in the G-O/DMF dispersion (exfoliated at 0.5 mg/ml), with a large distribution of lateral dimensions.

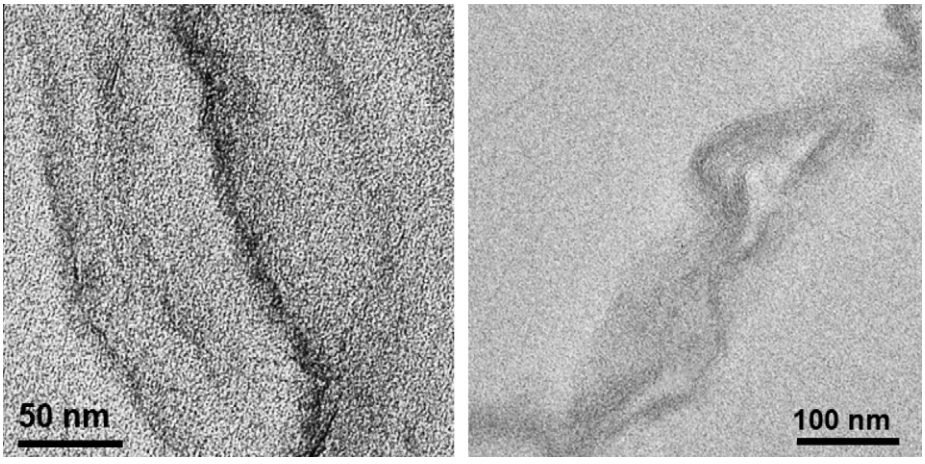

Fig. 2 – TEM images of (a) 0.5 wt.% RG-O in PMMA and (b) 4 wt.% RG-O in PMMA, showing the presence of multi-layer platelets with a crumpled morphology.

corresponding to the interlayer spacing of graphite oxide, suggesting an exfoliated morphology of both types of CMG platelets in PMMA across all loadings. However, the lack of a diffraction peak in the XRD pattern does not necessarily suggest the absence of stacked platelets [9], as confirmed by our TEM observations. This is likely because the relatively low volume percent of filler (approximately 4 vol.% at the highest loading)—a fraction of which may exist as multi-layer stacks—contributes little to the scattering signal relative to the PMMA matrix. Additionally, we analyzed the fracture surfaces of the composites using SEM. We attempted to examine the fracture surface for the presence of 'filler pull-out,' as has been previously reported as evidence for matrix-filler interfacial adhesion for thermally-exfoliated graphite oxide/PMMA composites [21]. However, PMMA is an insulating polymer and charging on the surface of the composite prevented

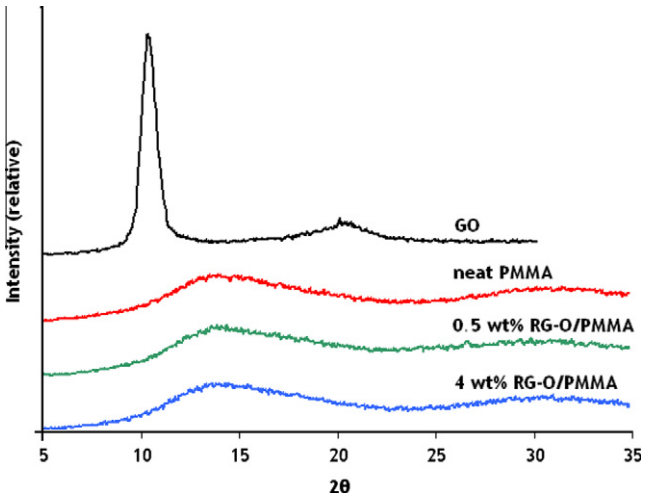

Fig. 3 – Wide angle X-ray scattering patterns for the composites. No presence of layered GO was detected at any loading, suggesting an exfoliated morphology in the composites.

resolution of the cross section down to the platelet level in our study. Qualitative observations made of the fracture surface at lower magnifications suggested a cup-cone fracture mechanism for neat PMMA versus the composites, which all showed brittle fracture surfaces (figures provided in Supplementary Information, Fig. S3).

Results from DMA experiments on the G-O/PMMA and RG-O/PMMA composites indicate that the glass transition temperatures (T_g) of the composites are increased substantially relative to neat PMMA. The modulus values also show increases compared with neat PMMA, indicating reinforcement (see Fig. 4), which is consistent with results from tensile testing (presented below). The RG-O/PMMA composites show shifts in T_g of more than 15 °C at loadings down to 0.05 wt.%, with only small increases in T_g beyond this loading (see Supplementary Information, Table S1). Notably, an increase in the area under the loss peak (E'') was observed at higher loadings, possibly suggesting increased segmental mobility in the composites at T_g versus neat PMMA. Large shifts in the T_g of PMMA at low loadings of graphene-based filler have been reported elsewhere [21]. While our study achieved a similar onset of a large T_g shift to previous work on thermally-exfoliated graphite oxide/PMMA composites [21], the incremental changes in T_g were much lower in this study. Moreover, even after numerous attempts, the large shifts in T_g observed by DMA were not replicated using DSC.

The origin of such T_g shifts has been attributed to the presence of so-called 'interphase' polymer, which arises due to the interaction of the chains with the platelet surface [22–26]. In our system, in which attractive interactions between the polar functional groups of G-O (or residual functional groups of RG-O) and PMMA may exist, chains several nanometers away from the platelet surface may have restricted mobility, creating an enormous volume of matrix polymer with increased T_g [25]. Percolation of this network of interphase polymer could then manifest the large T_g shift of the bulk composite.

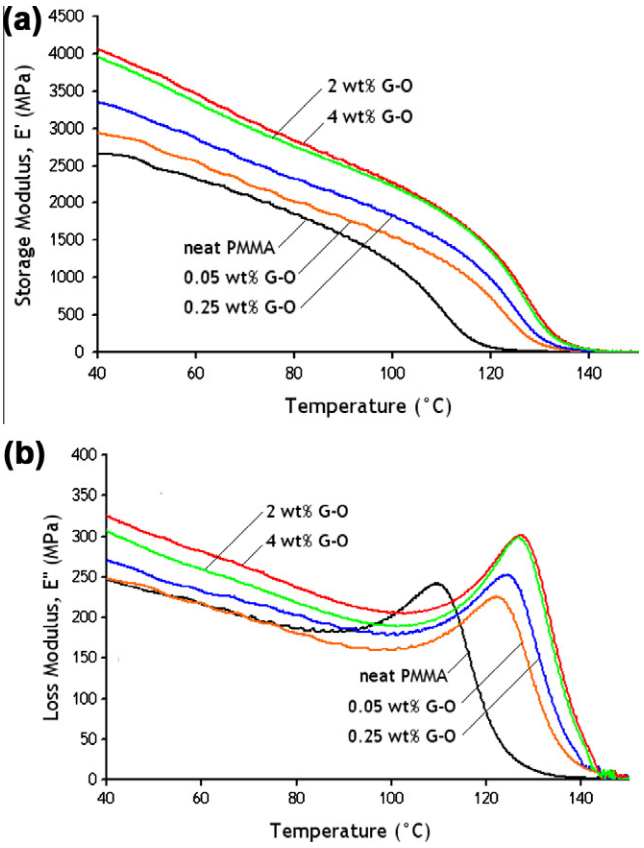

Fig. 4 – (a) Storage modulus and (b) loss modulus versus temperature for neat PMMA and G-O/PMMA composites as measured by DMA.

G-O and RG-O platelets were found to have a significant reinforcing effect at low loadings, which tapered off at higher loadings. Table 1 summarizes all data obtained from tensile testing, and Fig. 5 plots the modulus of the composites as a function of filler loading. For reference, the experimental data is compared with modulus predictions based on Mori–Tanaka theory [27,28] (details on this calculation are in Supplementary Information), which assumes unidirectional, ellipsoidal platelets and neglects possible contribution of the interphase [29]. Modulus values measured (by AFM tip-induced deformation) for G-O platelets range from approximately 208 GPa [30] up to 650 GPa [31] while RG-O platelets have been measured to have a modulus of 250 GPa [31]. Assuming a value of approximately 250 GPa for both types of CMG platelets, it can be seen from Fig. 5 that an effective platelet aspect ratio (A_f) of 100 captures the trend in modulus increase quite well up to 1 wt.%. However, a significant deviation is apparent at higher loadings. This deviation may be due to agglomeration of filler, which was observed in the TEM analysis (but not by XRD, as shown in Fig. 3). Thus, our data in conjunction with Mori–Tanaka theory is evidence for a good dispersion at lower loadings ($A_f > 100$ assuming a platelet modulus of 250 GPa) which progressively worsens as loading increases (A_f decreasing to approximately 30 at 4 wt.% loading).

While both types of composites showed similar increases in elastic modulus, the tensile strength of the G-O/PMMA composites was markedly higher than the RG-O/PMMA

Table 1 – Results of the tensile testing experiments (three samples were tested at each loading).

	E (GPa)	% Change, E	σ (MPa)	% Change, σ
RG-O (wt.%)				
0	3.43 ± 0.06	–	58.1 ± 1.95	–
0.25	3.75 ± 0.57	9.5	59.5 ± 4.25	2.4
0.5	4.04 ± 0.22	17.8	59.0 ± 4.75	1.5
1	4.28 ± 0.17	25.0	53.0 ± 5.55	−8.8
2	4.65 ± 0.35	35.8	57.0 ± 4.55	−1.9
4	4.56 ± 0.18	33.0	48.9 ± 1.15	−15.8
G-O (wt.%)				
0.25	3.65 ± 0.06	6.4	62.1 ± 0.60	6.9
0.5	4.19 ± 0.03	22.2	66.4 ± 1.75	14.3
1	4.39 ± 0.18	28.3	70.9 ± 0.15	22.0
2	4.45 ± 0.00	29.9	66.8 ± 3.05	15.0
4	4.53 ± 0.32	32.3	65.4 ± 5.35	12.6

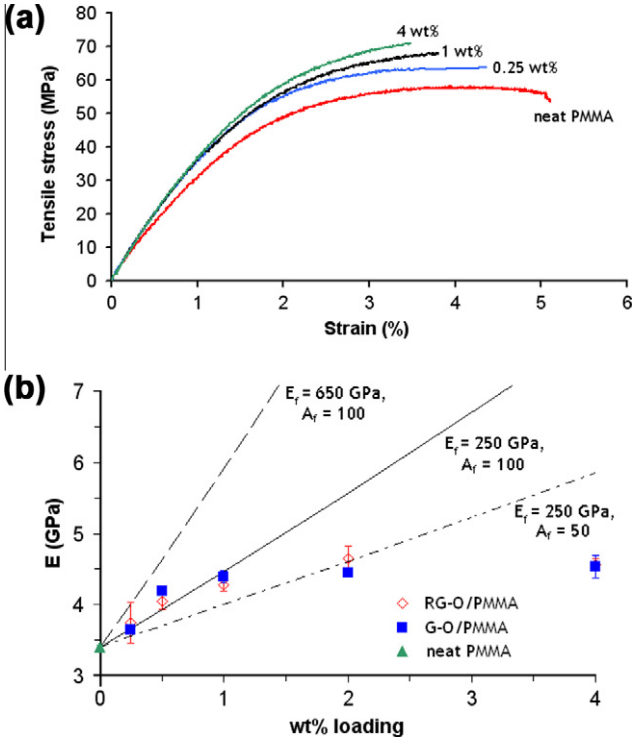

Fig. 5 – (a) Representative stress–strain curves of the composites (with G-O filler) and (b) average modulus values for G-O and RG-O-filled composites, plotted versus theoretical modulus values predicted by Mori–Tanaka theory, using various values for the platelet modulus (E_f) and aspect ratio (A_f).

composites—while G-O produced increases in tensile strength of more than 20%, RG-O, on average, caused the tensile strength of the composite to decrease versus neat PMMA. Since both G-O and RG-O/PMMA composites showed similar dispersions of filler (at lower loadings) by TEM and XRD analysis, this difference could perhaps be due, at least in part, to the higher presence of polar functional groups (e.g., hydroxyl, epoxide, and carboxylic acid groups) on the platelet surface, which might facilitate better interfacial adhesion between G-O and PMMA versus RG-O. Notably, injection molded samples were briefly subjected to compounding prior to molding; however, this was found to cause no discernable effect on the dynamic mechanical properties or on the dispersion based on a WAXS study. Representative stress–strain curves of G-O/PMMA composites, along with neat PMMA, are provided in Fig. 5. Elongation at break was observed to decrease with increasing weight fraction of both types of filler, consistent with the more brittle fracture surfaces observed by SEM.

Electrically conductive polymer composites with graphene-based fillers have been reported for a variety of systems [2], occasionally at low loadings of filler, such as 0.2 wt.% as reported for a CMG/polystyrene composite [16]. Electrically conductive PMMA matrix composites with graphene-based fillers have also been reported [17,32]. In this study, however, no major conductivity increase was observed at any loading. Indeed, at all loadings of both G-O and RG-O (for both hot pressed and injection molded specimens), the conductivity remained sufficiently low such that it could not be determined with our four-probe measurement setup (detection threshold: 200 GΩ). Thus, no conductivity values and no electrical percolation threshold could be determined for this composite system.

CMG fillers have been widely reported to improve the thermal stability of polymer composites relative to the host polymer [2,3]. Non-oxidative thermal degradation studies of the composites were performed using thermogravimetric analysis (TGA). The results are shown in Fig. 6, where the shift in the onset of the thermal degradation temperature with weight percent loading of CMG is illustrated. Both G-O and RG-O-filled composites showed similarly significant improvements in the non-oxidative thermal stability compared with neat PMMA.

Attempts were made to characterize any change in polymer structure with CMG loading to investigate whether the property improvements of the composites were influenced by possible changes in polymer structure, due to the presence of G-O platelets during polymerization. As shown in Fig. 7, no change in the NMR spectrum was observed between neat PMMA and the composites. GPC measurements indicated that the molecular weight of the composites increased slightly with higher loadings of CMG filler (Table 2). Both ^{1}H and ^{13}C solution NMR revealed that the dominant triad tacticity of

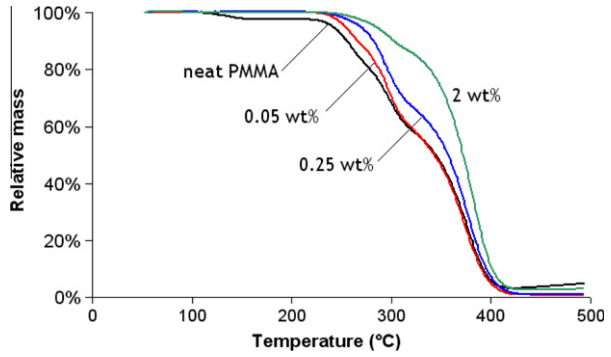

Fig. 6 – TGA curves for the RG-O composites versus neat PMMA, showing increased thermal stability with loading of RG-O. Similar trends were observed for G-O/PMMA composites.

the PMMA to be rr (syndiotactic), and tacticity of the PMMA was found to be the same for the neat, and 8 wt.% RG-O/PMMA and 8 wt.% G-O/PMMA samples, indicating no change in tacticity with loading of CMG filler (Table 3). No presence of the G-O was detected in the NMR spectra. Cross-polarization (CP) buildups from solid state ^{13}C CP MAS NMR measurements were used to extract the relaxation parameter T_{CH} (carbon–proton interaction) to probe changes in the low-frequency polymer relaxation dynamics with filler loading at temperatures well below the T_g of PMMA (Supplementary Information; Table S1 and Fig. S5). The most pronounced changes in polymer dynamics were observed at low G-O and RG-O content (0.05 wt.%), while the dynamics began to revert back to neat PMMA between 2 and 4 wt.% for both fillers. We speculate that these results reflect increasing aggregation of the platelets at higher loading as indicated by the changes in mechanical properties.

Table 3 – Tacticity ratios for neat, 8 wt.% G-O/PMMA and 8 wt.% RG-O/PMMA samples based on integration of the carbonyl region in the ^{13}C NMR solution spectra.

Sample ID	(rr)%	(mr)%	(mm)%
Neat PMMA	59.6	37.1	3.3
8 wt.% G-O/PMMA	56.9	39.0	4.1
8 wt.% RG-O/PMMA	60.2	35.3	4.3

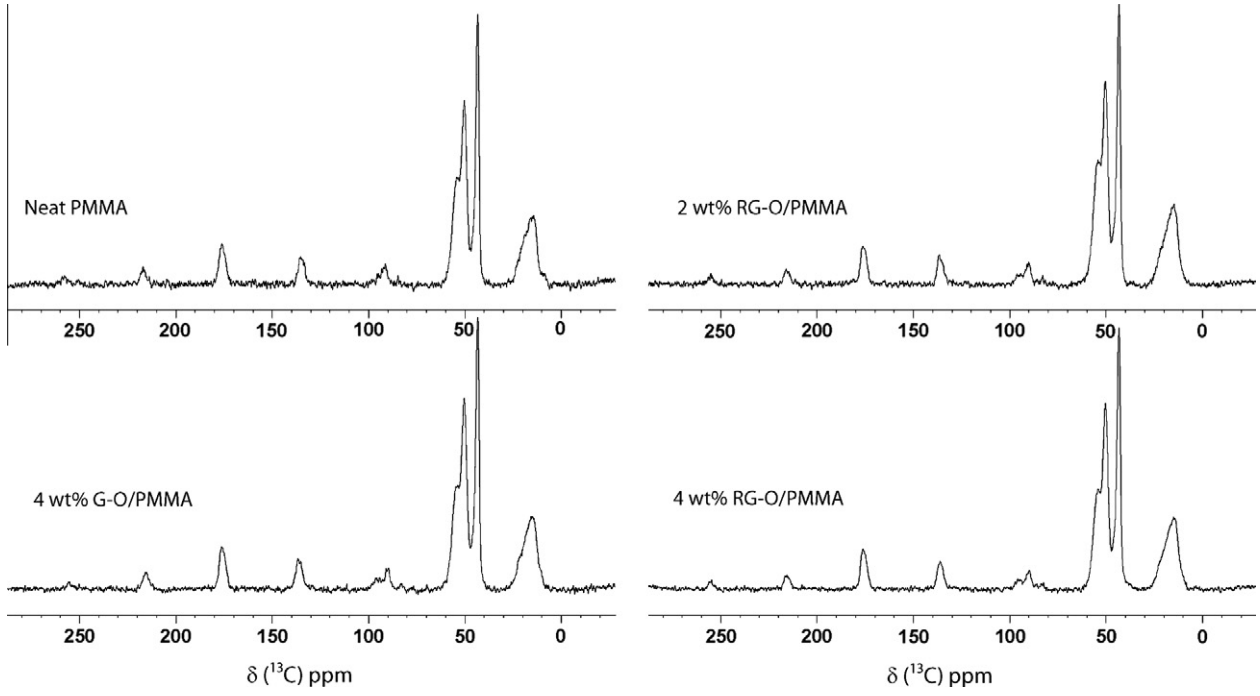

Fig. 7 – Representative solid state ^{13}C CPMAS NMR spectra of the PMMA composites (asterisks indicate spinning sidebands).

Table 2 – Molecular weight and polydispersity index of the neat PMMA and composites at various loadings, as measured by gel permeation chromatography.

Sample	M_w	M_w/M_n
Neat PMMA	200,900	2.06
0.05 wt.% G-O/PMMA	187,500	2.09
0.25 wt.% G-O/PMMA	191,600	2.17
1 wt.% G-O/PMMA	179,500	1.71
2 wt.% G-O/PMMA	217,400	2.38
8 wt.% G-O/PMMA	280,600	1.76

4. Conclusions

We prepared composites of PMMA with two types of CMG materials as filler: graphene oxide (G-O) and reduced graphene oxide (RG-O). The composites were prepared using an *in situ* polymerization method and processed using microcompounding/injection molding or hot pressing. Injection molded samples were subjected to standard tensile testing and showed increases in modulus for both CMG/PMMA composites, but only increases in strength for G-O in PMMA. Increases in the dynamic modulus were observed by DMA, where we also observed shifts of over 15 °C in T_g versus neat PMMA. Spectroscopic studies using FT-IR and NMR along with GPC revealed no evidence of variation in the structure of the polymer with increased CMG loading. The results indicate that both RG-O and G-O fillers provide substantial property improvements relative to neat PMMA, although this study suggests that G-O platelets offer the advantage of increased tensile strength whereas RG-O platelets do not. Mori–Tanaka theory suggests a good dispersion of filler at lower loadings (up to 1 wt.%), which progressively worsens at higher loadings. Based on TEM observations and solid state NMR studies, we believe this is due to agglomeration of the platelets (whether due to incomplete exfoliation and/or platelet restacking) at higher loadings.

Acknowledgements

The authors would like to thank Prof. Don Paul for use of the melt compounding and injection molding equipment, Prof. Ken Liechti for use of mechanical testing equipment, and Prof. Chris Bielawski for use of the GPC and IR spectrometer. This work was supported (in part) by the Laboratory Directed Research and Development (LDRD) program and the National Institute for Nano-Engineering at Sandia National Laboratories. Sandia National Laboratories is a multi-program laboratory operated by Sandia Corporation, a wholly owned subsidiary of Lockheed Martin company, for the US Department of Energy's National Nuclear Security Administration.

Appendix A. Supplementary data

Supplementary data associated with this article can be found, in the online version, at doi:10.1016/j.carbon.2011.02.023.

REFERENCES

[1] Zhu Y, Murali S, Cai W, Li X, Suk JW, Potts JR, et al. Graphene and graphene oxide: synthesis, properties, and applications. Adv Mater (Weinheim, Germany) 2010;22:3906–24.
[2] Potts JR, Dreyer DR, Bielawski CW, Ruoff RS. Graphene-based polymer nanocomposites. Polymer 2011;52:5–25.
[3] Kim H, Abdala AA, Macosko CW. Graphene/polymer nanocomposites. Macromolecules 2010;43:6515–30.
[4] Dreyer DR, Park S, Bielawski CW, Ruoff RS. The chemistry of graphene oxide. Chem Soc Rev 2010;39(1):228–40.
[5] Park S, Ruoff RS. Chemical methods for the production of graphenes. Nat Nanotechnol 2009;5(4):217–24.
[6] Park S, An JH, Jung IW, Piner RD, An SJ, Li XS, et al. Colloidal suspensions of highly reduced graphene oxide in a wide variety of organic solvents. Nano Lett 2009;9(4):1593–7.
[7] Schniepp HC, Li JL, McAllister MJ, Sai H, Herrera-Alonso M, Adamson DH, et al. Functionalized single graphene sheets derived from splitting graphite oxide. J Phys Chem B 2006;110(17):8535–9.
[8] Zhu YW, Murali S, Stoller MD, Velamakanni A, Piner RD, Ruoff RS. Microwave assisted exfoliation and reduction of graphite oxide for ultracapacitors. Carbon 2010;48(7):2118–22.
[9] Kim H, Macosko CW. Morphology and properties of polyester/exfoliated graphite nanocomposites. Macromolecules 2008;41(9):3317–27.
[10] Kim H, Macosko CW. Processing-property relationships of polycarbonate/graphene composites. Polymer 2009;50(15):3797–809.
[11] Kim H, Miura Y, Macosko CW. Graphene/polyurethane nanocomposites for improved gas barrier and electrical conductivity. Chem Mater 2010;22(11):3441–50.
[12] Moon IK, Lee J, Ruoff RS, Lee H. Reduced graphene oxide by chemical graphitization. Nat Commun. doi: 10.1038/ncomms1067.
[13] Stankovich S, Piner RD, Chen X, Wu N, Nguyen SBT, Ruoff RS. Stable aqueous dispersions of graphitic nanoplatelets via the reduction of exfoliated graphite oxide in the presence of poly(sodium 4-styrenesulfonate). J Mater Chem 2006;16:155–8.
[14] Stankovich S, Dikin DA, Piner RD, Kohlhaas KA, Kleinhammes A, Jia Y, et al. Synthesis of graphene-based nanosheets via chemical reduction of exfoliated graphite oxide. Carbon 2007;45(7):1558–65.
[15] Li D, Muller MB, Gilje S, Kaner RB, Wallace GG. Processable aqueous dispersions of graphene nanosheets. Nat Nanotechnol 2008 Feb;3(2):101–5.
[16] Stankovich S, Dikin DA, Dommett GHB, Kohlhaas KM, Zimney EJ, Stach EA, et al. Graphene-based composite materials. Nature 2006;442(7100):282–6.
[17] Jang JY, Kim MS, Jeong HM, Shin CM. Graphite oxide/poly(methyl methacrylate) nanocomposites prepared by a novel method utilizing macroazoinitiator. Compos Sci Technol 2009;69(2):186–91.
[18] Paul DR, Robeson LM. Polymer nanotechnology: nanocomposites. Polymer 2008;49(15):3187–204.
[19] Hummers WS, Offeman RE. Preparation of graphitic oxide. J Am Chem Soc 1958;80(6):1339.
[20] Paredes JI, Villar-Rodil S, Martinez-Alonso A, Tascon JMD. Graphene oxide dispersions in organic solvents. Langmuir 2008;24(19):10560–4.
[21] Ramanathan T, Abdala AA, Stankovich S, Dikin DA, Herrera-Alonso M, Piner RD, et al. Functionalized graphene sheets for polymer nanocomposites. Nat Nanotechnol 2008 Jun;3(6):327–31.
[22] Bansal A, Yang H, Li C, Cho K, Benicewicz BC, Kumar SK, et al. Quantitative equivalence between polymer nanocomposites and thin polymer films. Nat Mater 2005;4(9):693–8.
[23] Ellison CJ, Torkelson JM. The distribution of glass-transition temperatures in nanoscopically confined glass formers. Nat Mater 2003;2(10):695–700.
[24] Priestley RD, Ellison CJ, Broadbelt LJ, Torkelson JM. Structural relaxation of polymer glasses at surfaces, interfaces, and in between. Science 2005;309(5733):456.
[25] Qiao R, Brinson LC. Simulation of interphase percolation and gradients in polymer nanocomposites. Compos Sci Technol 2009;69(3–4):491–9.
[26] Rittigstein P, Priestley RD, Broadbelt LJ, Torkelson JM. Model polymer nanocomposites provide an understanding of

confinement effects in real nanocomposites. Nat Mater 2007;6(4):278–82.
[27] Mori T, Tanaka K. Average stress in matrix and average elastic energy of materials with misfitting inclusions. Acta Metall 1973;21:571–4.
[28] Tandon GP, Weng GJ. The effect of aspect ratio of inclusions on the elastic properties of unidirectionally aligned composites. Polym Compos 1984;5:327–33.
[29] Fornes TD, Paul DR. Modeling properties of nylon 6/clay nanocomposites using composite theories. Polymer 2003;44(17):4993–5013.
[30] Suk JW, Piner RD, An J, Ruoff RS. Mechanical properties of monolayer graphene oxide. ACS Nano. 2010;4:6557–64.
[31] Gómez-Navarro C, Burghard M, Kern K. Elastic properties of chemically derived single graphene sheets. Nano Lett 2008;8(7):2045–9.
[32] Chen G, Weng W, Wu D, Wu C. PMMA/graphite nanosheets composite and its conducting properties. Eur Polym J 2003;39(12):2329–35.